Chapter 5
ROLE OF CHEMICAL PRESSURE UPON THE ELECTRONIC STRUCTURE OF $Ho_2Ge_xTi_{2-x}O_7$

5.1 Introduction

Considering the influence of chemical pressure on the magnetic properties and having a widely different crystal structure for germanates, it is vital to investigate the role of chemical pressure upon the electronic structure of $Ho_2Ge_xTi_{2-x}O_7$ and its associated optical properties. After studying the spin dynamics of these magnetically frustrated systems and establishing the robustness of the ice-like spin freezing mechanism in $Ho_2Ti_2O_7$, we tried to look for its applications in relevance to devices and explored its optical and electronic properties. The electronic levels, band structure, and density of states had been theoretically verified through density functional theory (DFT) calculations. An attempt to appraise the relationship between structural, optical, and electronic properties of $Ho_2Ge_xTi_{2-x}O_7$ series to bridge the knowledge gap is described below.

In this chapter we present a detailed theoretical and experimental analysis of electronic structure investigation of $Ho_2Ge_xTi_{2-x}O_7$ (x = 2, 1.9, 1.75, 1.5 1, 0.5, 0.25, 0.1, and 0) series. The coexistence of Ti^{4+} and Ge^{4+} along with rare earth element and oxygen in this composition makes these materials extremely interesting from the point of view of the fundamental problem regarding energy band structure in solid-state physics.

Spectroscopic techniques and computational approach had been applied to study the electronic structure of Valence Band (V.B.) and Conduction Band (C.B.), Band gap energy (E_g), orbitals involved in hybridization, influence of the crystal structure, and effect of chemical pressure on the electronic subsystem. The band gap value of these systems puts them in insulator class of materials and could be efficiently exploited for various applications where optical and magnetic properties are combined. In this series, a subtle difference in the Ho^{+3} states due to chemical pressure effects has been exhibited through the complex pattern of absorption and emission spectra. A high probability of 4f-4f forbidden optical transitions present in these systems suitably places them in the category of materials for quantum information storage and biological imaging applications.

5.2 Structural analysis of $Ho_2Ge_xTi_{2-x}O_7$

Nemoshkalenko *et al.* reported the electronic structure of $A_2Ti_2O_7$ mentioning that the optical band gap of these systems is related with the degree of distortion created in the TiO_6 octahedron. The degree of distortion is directly reflected with the change in the value of "***x***" parameter i.e., the refinable parameter as mentioned in the **Table 5.1.**

Table 5.1 The "*x*" parameters for $A_2Ti_2O_7$ (A = Sm-Lu), the variation created a change in the band gap values. [93]

Compound	a_0 ***(Å)***	***x***	$d_{R-O'}$	d_{R-O}	d_{Ti-O}
$Sm_2Ti_2O_7$	10.233	0.327	2.216	2.531	1.973
$Eu_2Ti_2O_7$	10.196	0.327	2.208	2.522	1.966
$Gd_2Ti_2O_7$	10.185	0.322	2.205	2.555	1.944
$Tb_2Ti_2O_7$	10.152				
$Dy_2Ti_2O_7$	10.124	0.323	2.192	2.533	1.936
$Ho_2Ti_2O_7$	10.100				
$Er_2Ti_2O_7$	10.087	0.331	2.184	2.467	1.961
$Yb_2Ti_2O_7$	10.030				
$Lu_2Ti_2O_7$	10.018	0.330	2.169	2.441	1.944

As could be seen from table, changing the element at A site from Sm to Lu i.e., by varying the chemical pressure the authors had been successful in tuning the band gap as shown in **Figure 5.1**.

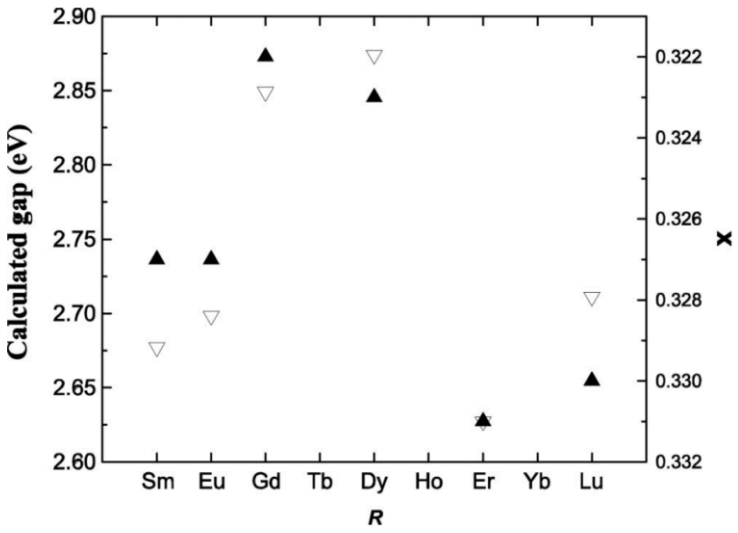

Figure 5.1 Calculated optical band gap values (open down triangles) and distortion parameter x (solid up triangles). [93]

As described in the chapter 1, the descriptive formula of $Ho_2Ti_2O_7$ can be written as $Ho_2Ti_2O_6O'$ because six O anions possessing point symmetry C_{2v} at 48f Wyckoff site with (***x, 1/8, 1/8***) coordinates are equivalent whereas the seventh O' having point symmetry T_d at 8b Wyckoff site (***3/8, 3/8, 3/8***) has a distinct position in the structure. Ho^{3+} and Ti^{4+} occupy point symmetry D_{3d} having Wycoff positions 16d (***½, ½, ½***) and 16c (***0, 0, 0***), respectively. The Ho^{3+} cation inside oxygen scalenohedra is eight coordinated (6O + 2O'). The Ti^{4+} cation with 6 O^{2-} ions form trigonal antiprisms as Ti^{4+} lies within TiO_6 octahedron. Both 16c and 16d sites form three dimensional array of corner-sharing tetrahedron, giving rise to one of the canonical geometrically frustrated lattices [20].

Detailed investigation of the crystallographic structure of $Ho_2Ge_2O_7$ shows that seven pyro-oxygens form a polyhedron; as such, it possesses non centro-symmetric distorted pentagonal bipyramidal structure with Ho-O coordination revealing a spiral of alternating edge and corner-sharing triangles; as already discussed in chapter 4 [28]. The distortion of the GeO_4 tetrahedron and HoO_7 coordination polyhedron upon B site substitution makes the explanation of crystal field effect of $Ho_2Ge_2O_7$, quite difficult.

HRXRD for $Ho_2Ge_xTi_{2-x}O_7$ sample series (x = 0, 0.1, 0.25, 0.5, 1, 1.25, 1.5, 1.9 and 2) was obtained. x = 0, 0.1, and 0.25 crystallizes in cubic structure ($Ho_2Ti_2O_7$) along with significant distortion for x = 0.1 and 0.25. x = 2 crystallizes in tetragonal phase with few unidentified peaks, followed by the coexistence of both cubic (Fd-3m) and distorted cubic/tetragonal phases ($P4_12_12$) for x = 1.9, 1.75, 1.5, and 0.5 along with some other unidentified crystallographic phases too. There exist structural changes related to the increasing inclusion of smaller Ge^{4+} cation replacing Ti^{4+} (ionic radii of Ge^{4+} in 6 coordination state = 67 pm and that of Ti^{4+} in 6 coordination state is 74.5 pm) at Ti site in $Ho_2Ti_2O_7$. Net decrease in the unit cell volume is expected. This decrease is reflected in $Ho_2Ge_xTi_{2-x}O_7$ lattice parameter from "*a"* = 10.1099(1)Å (x=0) to 10.0861(1) Å(x=0.25). Till x = 0.25, distortion accompanied in cubic phase has been retained. The theoretical lattice parameter for $Ho_2Ti_2O_7$ (x=0) obtained from DFT calculation turns out to be 9.8923 Å within less than 3% of the experimental value, showing excellent agreement with the experimental value. The refinable positional parameter of O (***x, 1/8, 1/8***) controls the local geometry around the Ho^{3+} site and it also estimates the distortion of the TiO_6 octahedron [94]. The value of ***"x"*** increases from 0.3308 (3) in $Ho_2Ti_2O_7$ to 0.3327 (1) in $Ho_2Ge_{0.25}Ti_{1.75}O_7$. The increase in the value of ***"x"*** is directly changing the geometrical constraints of the octahedron (trigonal antiprism) about 16c site (Ti

atom) as Ti-O bond length increases from 1.9650 (13) Å to 1.9682 Å with an increase in x in $Ho_2Ge_xTi_{2-x}O_7$ from 0 to 0.25. <Ho-O> distance also decreases, which is obvious since there is a direct correlation between <Ti-O> and <Ho-O> environment. The increase in <Ti-O> indicates the displacement of O atoms towards to Ho site. On the other hand, decreasing <Ho-O'> is essentially indicating the effect of distortion on the Ho site symmetry as well. The contraction in both Ho-O and Ho-O' bond length values from 2.4740(3) Å to 2.4552(1) Å and 2.1889(0) Å to 2.1837(0) Å respectively shows distinct shrinking effect behavior since the decrease in <Ho-O> also causes O-Ho-O' bond angle to decrease from 79.01(6) ° in $Ho_2Ti_2O_7$ to 78.79(6) ° in $Ho_2Ge_{0.25}Ti_{1.75}O_7$. This might be because shrinkage affecting one of the sub-network results in the displacement of the O'^{2-} anion linked with Ho^{3+}. The structural distortion parameters, is listed in **Table 5.2**.

Table 5.2 Cubic phase composition along with structural distortion parameters i.e., bond length and bond angle of $Ho_2Ge_xTi_{2-x}O_7$ (x = 0, 0.1 and 0.25)

x	Theoretical Lattice Parameter (Å)	Experimental Lattice Parameter (Å)	Refinable Parameter	Bond length (Å)				Bond angle (˚)		
				Ho-O	Ho-O'	Ti-O	Ho-Ho	O-Ho-O'	O-Ho-O	O-Ti-O
0	9.8923	10.1099(1)	0.3308(3)	2.4740(3)	2.1889(0)	1.9650(2)	3.5744(0)	79.01(6)	63.55(4)	83.04(1)
0.1	9.8525	10.1036(1)	0.3310(1)	2.4610(3)	2.1875(0)	1.9710(2)	3.5722(1)	78.72(6)	63.73(4)	82.45(1)
0.25	9.7900	10.0861(1)	0.3327 (1)	2.4552(1)	2.1837(0)	1.9682(1)	3.5660(3)	78.79(6)	63.75(1)	82.59(1)

5.3 Electronic structure calculation through DFT calculations.

Theoretical approach was adopted to interpret the electronic structure of $Ho_2Ge_xTi_{2-x}O_7$ spin ice systems. We have extensively employed Local density approximation (LDA) and LDA – 1/2 within the DFT calculations to extract density of states and band structure.

5.3.1 Density of state (DOS) calculations of $Ho_2Ge_2O_7$

The density of state calculations was performed on this system for the acquaintance of the hybridized orbitals involved in the formation of the band structure. **Figure 5.2 (a)** and **Figure 5.2 (b)** show the partial DOS and total DOS of $Ho_2Ge_2O_7$ through LDA and LDA – 1/2 methods, respectively.

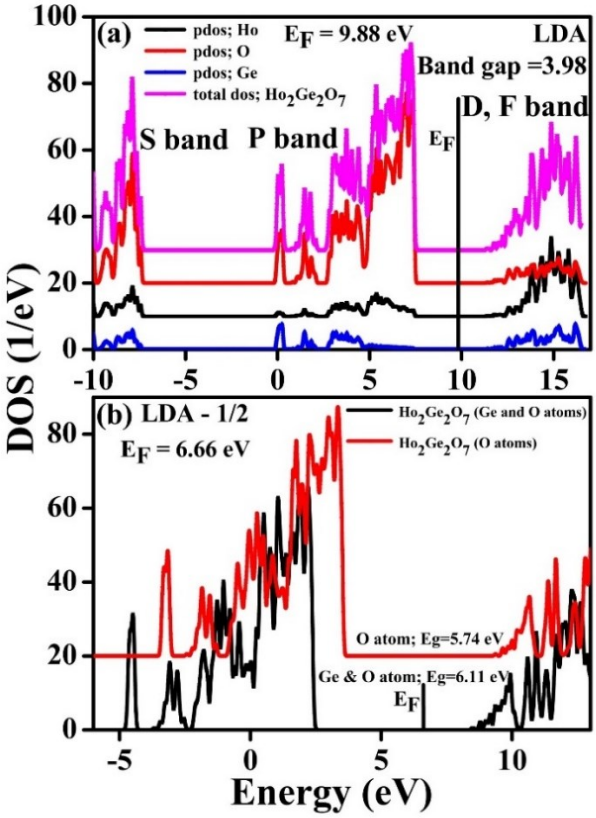

Figure 5.2 Density of States (DOS) of $Ho_2Ge_2O_7$ (a) Partial DOSs of Ho (6s, 5pand 5d); Ge (4s, 4p and 4d) and O (2s, 2p and 3d) states along with total DOS obtained from standard LDA and (b) total DOS from LDA half.

It indicates that the lower valence band is predominantly hybridized with O-2s, Ho-6s and Ge-4s states, whereas the upper valence band is dominated by O-2p, Ho-5p and Ge-4p states.

The conduction band is majorly formed by Ho-5d hybridized with Ge-4d and O-3d states. Despite that in $Ho_2Ge_2O_7$, the C.B. possess a partial fraction of all these Ge-4d, Ho-5d, and O-3d states, the transition at 240 nm (observed in the UV-Vis spectrum as will be shown in chapter 6) corresponding to band gap (~5.24 eV) can be attributed to electron transfer between Ge-4d and O-2p derived states.

5.3.2 Density of state calculations of $Ho_2Ti_2O_7$

Figure 5.3 (a) show the partial and total DOS obtained through LDA and **Figure 5.3 (b)** shows the total DOS of $Ho_2Ge_2O_7$ obtained through LDA–1/2 methods for $Ho_2Ti_2O_7$.

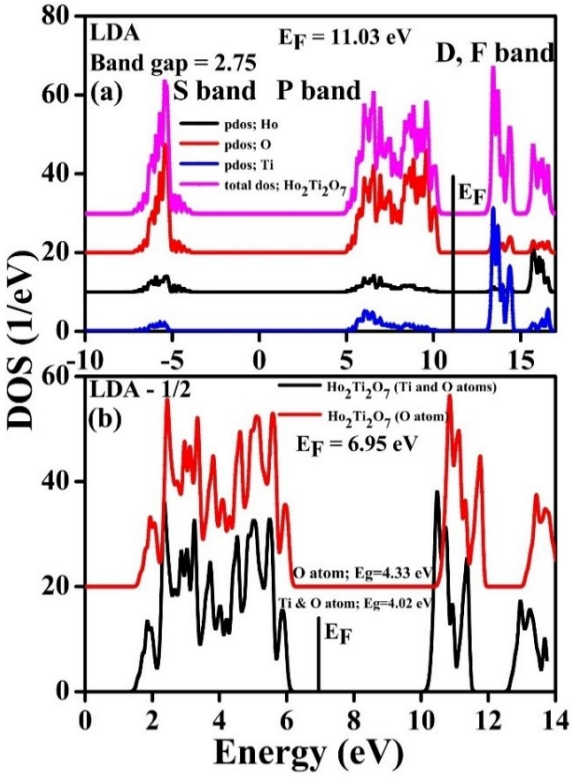

Figure 5.3 Density of States (DOS) of $Ho_2Ti_2O_7$ (a) Partial DOSs of Ho (6s, 5pand 5d); Ti (4s, 4p and 3d) and O (2s, 2p and 3d) states along with total DOS obtained from standard LDA (local density approximation) and (b) total DOS from LDA half involving self-energy correction method.

Here also, similar to $Ho_2Ge_2O_7$, the lower and upper valence band is predominantly contributed by O-2s states hybridized with Ho-6s and Ti-4s & O-2p states hybridized with Ho-5p and Ti-4p states, respectively. The conduction band primarily marks a dominant Ti-3d state separated with upper C.B. formed by Ho-5d state, and the relevance of this state will be discussed in the next section.

5.3.3 Evolution of total DOS for $Ho_2Ge_xTi_{2-x}O_7$

The evolution of total DOS of $Ho_2Ge_xTi_{2-x}O_7$ is shown in **Figure 5.4.** It indicates that V.B. edge is more sensitive than conduction band to composition. Partial DOS of $Ho_2Ti_2O_7$ displays a maximum cross-section of O-2p state in the vicinity of Fermi-level on V.B. side and that of the Ti-3d state in C.B. side. The states just above and below the gap is formed by O-2p state and Ti-3d state; hence electronic transition from O-2p (V.B.) to Ti-3d (C.B.) thus corresponds to band gap as shown in **Figure 5.3 (a)**. Also, the hybridization between O-2p and Ti-3d state is much stronger than the hybridization between Ho-5d and O-2p states. Ho-5d cross-section is very meagre as seen from partial DOS, but little overlapping of the Ho-5d and Ti-3d state suggests hybridization between these states in C.B. via O-2p electrons. Coming to **Figure 5.4 (a)**, Ge-3d state is manifested in DOS of $Ho_2Ge_2O_7$, immediate after the Ti substitution (x=1.75) at Ge site in $Ho_2Ge_2O_7$ increases the d state cross-section. This increase is assigned to the Ti-3d state, suggesting strong Ti-3d and O-2p bonding resulting in a stable Ti-d state in C.B that provides an explanation for the gradual decrease in the band gap energy with chemical pressure.

Increase in the hybridization cross-section of total DOS specifically of d-orbital of $Ho_2Ti_2O_7$ on Ge addition in C.B. is seen making the possibility of enhancement in the hybridization of

Ho-5d and O-2p states or Ti-3d and O-2p states. As shown in **Figure 5.4(b)** and **Figure 5.4 (c),** the Ti-3d state remains intact at fixed energy with increased Ge in $Ho_2Ge_xTi_{2-x}O_7$ and downshift in O-2p state in V.B. This suggests decreasing overlap between Ti-3d and O-2p state. The increase in Ti-O bond length due to octahedron distortion is responsible for the decreasing overlap between the Ti-3d and O-2p.

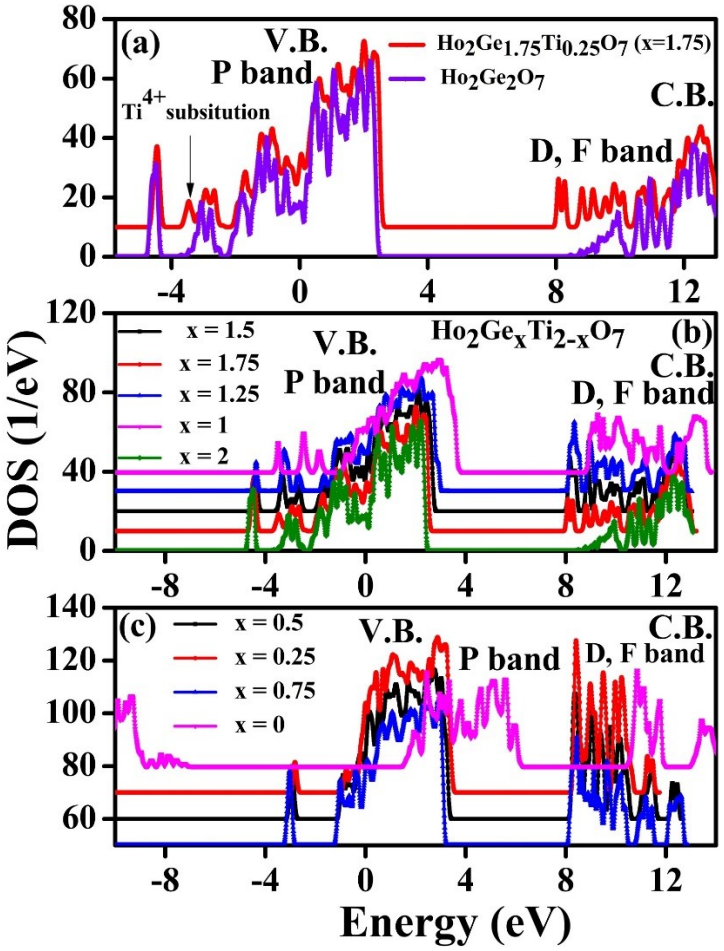

Figure 5.4 Total DOS of (a) $Ho_2Ge_2O_7$ along with B site Ti^{4+} substitution for x=1.75 ($Ho_2Ge_{1.75}Ti_{0.25}O_7$) (b) $Ho_2Ge_xTi_{2-x}O_7$ (x = 2, 1.75, 1.25, 1.5 and 1) and (c) $Ho_2Ge_xTi_{2-x}O_7$ (x = 0, 0.25, 0.5 and 0.75).

In $Ho_2Ge_2O_7$, state of C.B. is derived due to the overlapping of O-2p state with Ho-5d along with Ge-4d state. The Ge-4d state is shifted more towards the higher edge in the C.B. as displayed in both experimental (UV-Vis as shown in next chapter) and theoretical (band structure calculation as shown in next section) data resulting in its higher band gap value in comparison to $Ho_2Ti_2O_7$. The band gap obtained for all compositions is listed in **Table 5.3.**

Table 5.3 Band gap energies of $Ho_2Ge_xTi_{2-x}O_7$ (x = 2, 1.9, 1.75, 1.5, 1, 0.5, 0.25, 0.1 and 0) obtained from theoretical data (DFT calculations).

Compound	Band gap (eV); theoretical
$Ho_2Ge_2O_7$	6.11
$Ho_2Ge_{1.9}Ti_{0.1}O_7$	5.89 (estimated)
$Ho_2Ge_{1.75}Ti_{0.25}O_7$	5.52
$Ho_2Ge_{1.5}Ti_{0.5}O_7$	5.39
$Ho_2Ge_1Ti_1O_7$	5.06
$Ho_2Ge_{0.5}Ti_{1.5}O_7$	4.91
$Ho_2Ge_{0.25}Ti_{1.75}O_7$	4.85
$Ho_2Ge_{0.1}Ti_{1.9}O_7$	4.34 (estimated)
$Ho_2Ti_2O_7$	4.02

5.3.4 Band structure of $Ho_2Ge_2O_7$

The calculated band structure of tetragonal $Ho_2Ge_2O_7$ with phonon modes involved along the high symmetry point of the Brillouin zone using LDA method is shown in **Figure 5.5 (a).** The calculated band gap of $Ho_2Ge_2O_7$ is 3.98 eV. This theoretical value is much less than the experimental value of 5.2 eV obtained from UV-Vis data. At the valence band edge, the Γ and X point lie very close at a difference of 25 meV, but the direct band gap transition corresponds to Γ to Γ point. Since the band gap does not reasonably agree with the

experimental value, we preceded using LDA – 1/2 method. LDA – 1/2 calculations involve the electronic self-energy contribution [95] into the particle excitation energy in LDA, thus giving better results in band gap calculation of insulators. Using this method where both electron densities at Ge and O sites were considered, the obtained value of band gap for the same system is 6.12 eV (involving an indirect transition between Γ to X symmetry points), as shown in **Figure 5.5 (b)**.

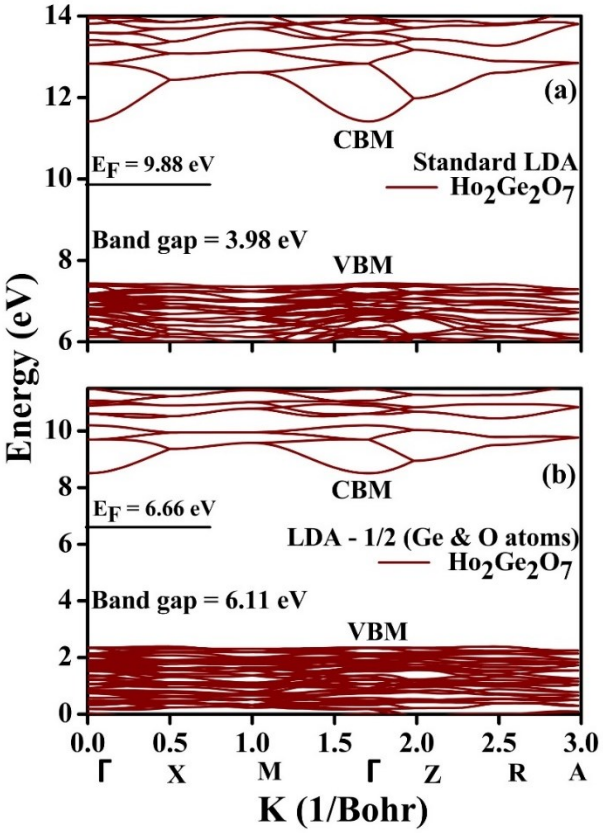

Figure 5.5 Band structure of $Ho_2Ge_2O_7$ obtained from (a) Standard LDA (local density approximation) having band gap of 3.98 eV with direct transition involving Γ symmetric point; (CBM – Conduction band minima; VBM – Valence band maxima) and (b) LDA half, (Ge and O atoms) involving self-energy correction method having band gap of 6.11 eV with indirect transition along Γ to X symmetry point of Brillouin zone.

The value obtained through LDA – 1/2 provides the basis for the explanation of the experimental band gap value obtained from UV-Vis data since these are highly correlated systems. **Table 5.4** shows energy involved in all the possible transitions (direct and indirect) along the symmetry points in $Ho_2Ge_2O_7$ tetragonal unit cell (**Figure 5.6**) through both LDA and LDA – 1/2 methods.

Table 5.4 Transitions involved along the symmetry points of the Brillouin zone in $Ho_2Ge_2O_7$ obtained from the band structure calculation through standard LDA and LDA – 1/2 (Ge and O atoms) method that involves self-energy correction.

x value	Coordinate	Symmetry point	Std. LDA				LDA1/2 (Ge and O atoms)			
			V.B. (eV)	C.B (eV)	Transition	Energy (eV)	V.B. (eV)	C.B (eV)	Transition	Energy (eV)
0	(0,0,0)	Γ	7.43	11.41	Γ⟶Γ	3.98	2.34	8.50	Γ⟶Γ	6.16
					Γ⟶Z	3.99			Γ⟶Z	6.16
					Γ⟶M	4.06			Γ⟶M	6.20
					Γ⟶R	4.00			Γ⟶R	6.12
					Γ⟶X	4.00			Γ⟶X	6.12
					Γ⟶A	4.11			Γ⟶A	6.26
0.5	(0,1/2,0)	X	7.41	12.43	X⟶X	5.02	2.38	9.36	X⟶X	6.98
1.0	(1/2,1/2,0)	M	7.35	12.61	M⟶M	5.26	2.30	9.57	M⟶M	7.27
1.7	(0,0,0)	Γ	7.43	11.41	Γ⟶Γ	3.98	2.34	8.50	Γ⟶Γ	6.16
1.9	(0,0,0.2)	Z	7.42	11.98	Z⟶Z	4.56	2.34	8.94	Z⟶Z	6.60
2.4	(0,0.5,0.2)	R	7.41	12.60	R⟶R	5.19	2.38	9.50	R⟶R	7.12
2.9	(0.5,0.5,0.2)	A	7.29	12.84	A⟶A	5.55	2.24	9.76	A⟶A	7.52

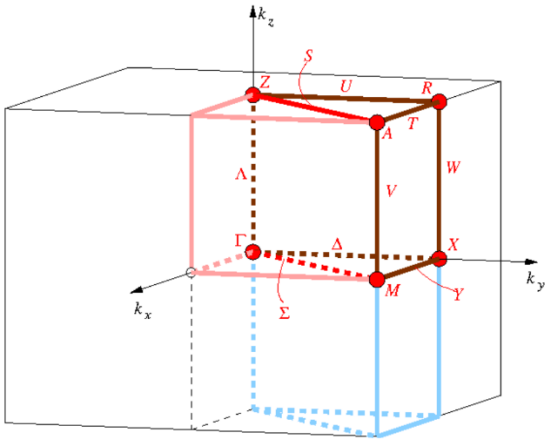

Figure 5.6 Symmetry points along with the phonons involved in indirect-transitions in the Brillouin zone for $Ho_2Ge_2O_7$ (space group; 92).

5.3.5 Band structure of $Ho_2Ti_2O_7$

Coming to the cubic system $Ho_2Ti_2O_7$, the direct band gap corresponding to Γ symmetry point transition is 2.73 eV through standard LDA calculations. The band structure obtained through LDA calculations is shown in **Figure 5.7 (a)**. When self-energy contribution of both Ti^{4+} and O^{2-} atoms is considered, the band gap value is 4.02 eV.

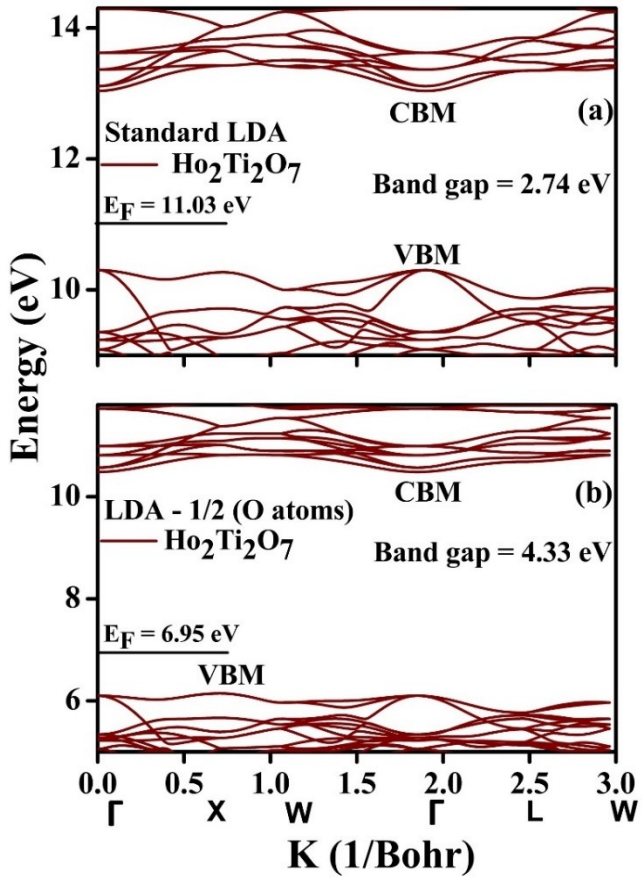

Figure 5.7 Band structure of $Ho_2Ti_2O_7$ obtained from (a) Standard LDA (local density approximation) having band gap of 2.74 eV with direct transition involving Γ symmetric point; (CBM – Conduction band minima; VBM – Valence band maxima) and (b) LDA half, (O atoms) involving self-energy correction method having band gap of 4.33 eV with indirect transition along Γ to X symmetry point of Brillouin zone.

This value is much closer to the experimental value of 3.74 eV obtained from Tauc plot (equation) of data obtained from UV-Vis absorption spectra as will be shown in next chapter. The earlier value of the experimental band gap of $Ho_2Ti_2O_7$ is 3.2 eV (reported by S.T. Bramwell et al.), and the theoretical value was 2.38 eV (obtained by H.Y Xiao)[53] [94]. The mismatch between both these previously reported values is about 1 eV. In this study, we obtained a more promising and agreed validation between the experimental and theoretical band gap for $Ho_2Ti_2O_7$ using LDA-1/2 approximation. If only O^{2-} site self-energy contribution was taken into account, the band gap value has been found to be 4.31 eV whereas it is 4.02 eV when both Ti^{4+} and O^{2-} sites are considered. This indicates again a strong electronic correlation between Ti-3d and O-2p states leading to the increased affinity in the band formation. The band structure using LDA – 1/2 methods is shown in **Figure 5.7 (b)**. All possible transitions involved along the Brillouin zone symmetry point of $Ho_2Ti_2O_7$ (**Figure 5.8**) has been shown in **Table 5.5**. The band gap energy of 4.31 eV corresponds to direct transition from Γ to Γ point.

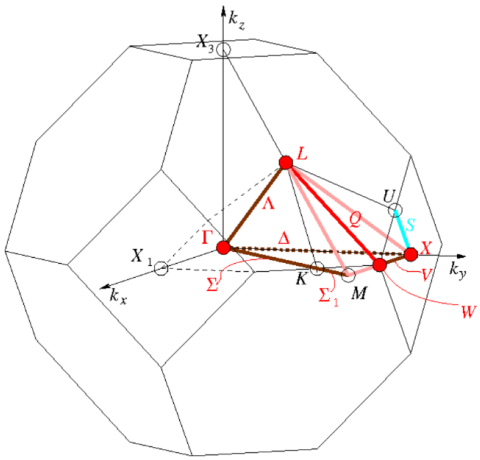

Figure 5.8 Symmetry points along with the phonons involved in indirect-transitions in the Brillouin zone for $Ho_2Ti_2O_7$ (space group; 227).

Table 5.5 Transitions involved along the symmetry points of the Brillouin zone in $Ho_2Ti_2O_7$ obtained from the band structure calculation through standard LDA and LDA – 1/2(O atoms) method that involves self-energy correction.

x value	Coordinate	Symmetry point	Std. LDA				LDA1/2 (Ge and O atoms)			
			V.B. (eV)	C.B (eV)	Transition	Energy (eV)	V.B. (eV)	C.B (eV)	Transition	Energy (eV)
0	(0,0,0)	Γ	10.3	13.03	Γ→Γ	2.73	6.09	10.4	Γ→Γ	4.31
					Γ→L	3.17			Γ→L	4.61
					Γ→W	3. 04			Γ→W	4.44
					Γ→X	2.83			Γ→X	4.26
0.7	(0,-0.5,0.4)	X	10.2	13.42	X→X	3.22	6.14	10.8	X→X	4.66
1.0	(-0.2,-0.4,0.6)	W	9.99	13.41	W→W	3.42	5.96	10.8	W→W	4.84
1.8	(0,0,0)	Γ	10.3	13.03	Γ→Γ	2.73	6.09	10.4	Γ→Γ	4.31
2.5	(0,0,0.6)	L	9.86	13.34	L→L	3.48	5.79	10.6	L→L	4.81
3.0	(-0.2,-0.4,-0.6)	W	9.99	13.41	W→W	3.42	5.96	10.8	W→W	4.84

5.4 Electronic structure analysis of $Ho_2Ge_xTi_{2-x}O_7$: experimental characterizations

One of the most powerful tools for the characterization of local electronic structure and electronic correlation effects is the XPS (x-ray photoelectron spectroscopy) and Ultraviolet photoelectron spectroscopy (UPS) experiments. This technique is based on the excitation of electrons from deeply bound core levels to unoccupied levels. The results of the electronic structure investigation for the compounds $Ho_2Ge_xTi_{2-x}O_7$ using XPS (core levels) and UPS (valence levels) studies had been presented. A good agreement between theoretical and experimental results were observed.

5.4.1 Ultraviolet photoelectron Spectroscopy

The hybridized states leading to band formation obtained through the theoretical calculation for $Ho_2Ge_2O_7$ has bene experimentally investigated through UPS measurements. The theoretically explained electronic states in previous section traces the origin of the four features marked as A, B, C, and D in experimental valence band spectra of $Ho_2Ge_2O_7$ obtained from UPS data. $Ho_2Ge_2O_7$ shows the dominance of O-2p state at -11.8 eV marked as A in **Figure 5.9 (a)**. Feature B centred at -8 eV belongs to Ge-4p state, and a small feature at -4 eV at C belongs to Ho 4f state.

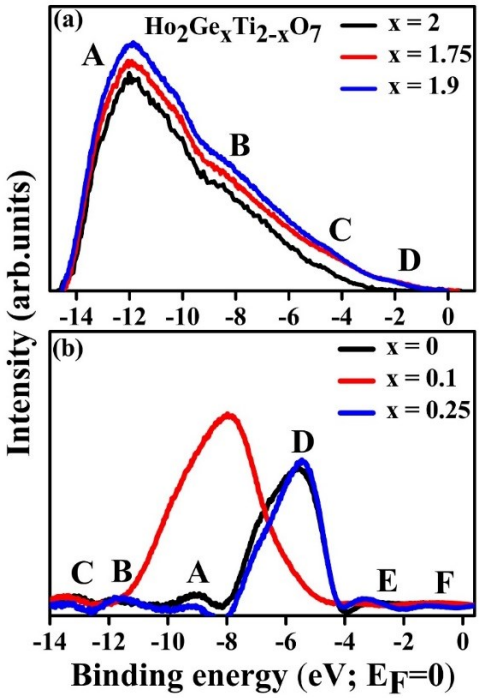

Figure 5.9 Valence band spectra of $Ho_2Ge_xTi_{2-x}O_7$ obtained from UPS spectra recorded at photon energy of 21.2 eV. (a) (x = 2, 1.9 and 1.75). Feature A marks the dominance of O-2p -11.8 eV), B; (Ge-4p at -8 eV), C; (Ho-4f at -4 eV) and D; (Ti-3d at 2 eV) state (b) (x = 0, 0.1 and 0.25). Feature A, B and C marks the hybridized s state of O, Ti and Ho at -9, -11 and -13 eV, D; (O-2p at -6 eV) and E and F; (Ho-4f at -4 eV). Positions have been designated according to the order of cross section assigned to these orbitals at hν = 1.2 eV.

These had been designated according to the order of cross-section assigned to these orbitals at a photon energy of 21.2 eV, having a value of 10.69 (O-2p), 1.528 (Ge-4p), and 0.9610 (Ho-4f) states [96]. The 4f state of Ho is the occupied orbitals shifted in the V.B. upon f-orbital splitting. With Ti substitution (x = 1.9) at Ge site, a small feature at -2 eV emerges corresponding to Ti-3d state, and this peak is manifested in UV-Vis absorption spectra (discussed in chapter 6) at 300 nm in $Ho_2Ti_2O_7$ and Ti^{4+} substituted $Ho_2Ge_2O_7$ for all x in $Ho_2Ge_xTi_{2-x}O_7$. The Ti-3d state is further confirmed from the prominence of cross section of D band in DOS plot for $Ho_2Ge_xTi_{2-x}O_7$ (for all x expect x =2) shown in **Figure 5.4 (b)**. This is a stable state responsible for the band gap in the Ti^{4+} substituted $Ho_2Ge_2O_7$ system. Ho, Ge, and O p orbital hybridized state initiating at 2.5 eV from the Fermi edge in UPS is also observed in DOS of $Ho_2Ge_2O_7$.

Six features identified in valence band spectra of $Ho_2Ti_2O_7$ are marked as A, B, C, D, E and F in **Figure 5.9 (b)**. In partial DOS of $Ho_2Ti_2O_7$ (**Figure 5.3 (a)**) we observe the s states hybridized centred at 17 eV from the Fermi level. Through UPS these hybridized states are manifested at features marked as A, B and C at -9, -11 and -13 eV from Fermi edge having very small cross sections using 21.2 eV of photon energy. The broad peak of D at -6 eV in UPS having maximum cross section of 10.69 corresponds to that of O-2p state. The broad feature from Fermi edge to -4 eV (E and F) belongs to Ho^{3+} 4f state (cross section = 0.961). These results for $Ho_2Ti_2O_7$ corroborate well with its DOS obtained through LDA – 1/2 calculations.

5.4.2 x-ray photoelectron spectroscopy

In order to get an insight of the core-level electronic interactions, x-ray photoelectron spectroscopy (XPS) has been performed on these systems. All the binding energy (B.E.) positions of states had been taken from the XPS data book [97] . XPS of $Ho_2Ge_xTi_{2-x}O_7$ is shown in **Figure 5.10 (a)** for x = 2, 1.9 and 1.75 and **Figure 5.10 (b)** for x = 0, 0.1 and 0.25. The strong interaction between the lower and upper valence band upon Ti substitution is also seen in the O-2s and Ho-5p core levels in the XPS spectra.

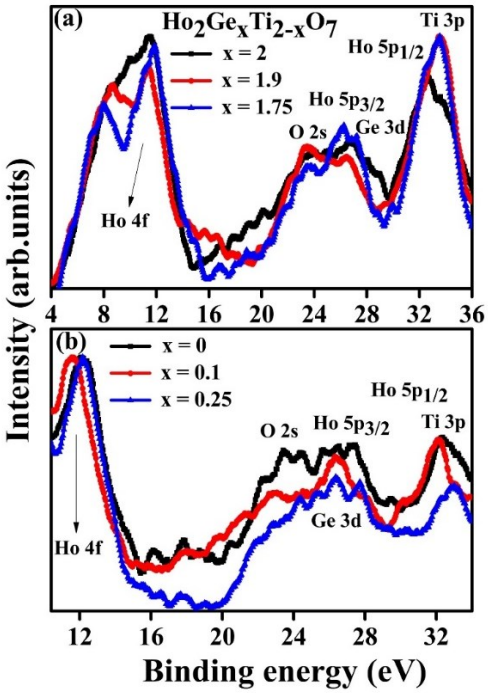

Figure 5.10 Core level spectra along with valence state of (a) $Ho_2Ge_xTi_{2-x}O_7$ (x = 2, 1.9 and 1.75) (b) $Ho_2Ge_xTi_{2-x}O_7$ (x = 0, 0.1 and 0.25) showing Ho 4f, $5p_{1/2}$, and $5p_{3/2}$; O 2s; Ge 3d and Ti 3p core and valence levels obtained from XPS.

The core-level features showed marked variation with the composition. $Ho_2Ti_2O_7$ displayed three sensitive features at energies centred at 11.6 eV, 25 eV, and 33 eV between 10-35 eV,

as shown in **Figure 5.10 (b)**. Notable intensity variation with chemical pressure is manifested by this system for features at 23 and 26 eV that indicates possible interactions between electrons of core levels. The 23 eV feature gets suppressed, whereas the feature at 26 eV is enhanced upon Ge^{4+} substitution at the Ti site. This intensity variation indicates the existence of a higher degree of interaction between the O-2s and Ho-5p or the formation of a chemical bond [93] between core level electrons of Ho-5p and O-2s orbitals upon Ge inclusion. As pointed out earlier, since Ho-O bond-length is larger than Ho-O', it can be easily inferred that there exists strong hybridization between Ho-5p and O'-2s state. $5p_{1/2}$ and $5p_{3/2}$ spin doublet components of Ho along with O-2s state lie in this binding energy range. Since the electronic binding energy of the Ho-$5p_{3/2}$ state is 26 eV, nearly equal to B.E. of electrons of the O'-2s state at 23 eV, these states are more likely to hybridize. Involvement of $5p_{1/2}$ electronic state is less likely because of its higher binding energy (30 eV). Further increase in Ge percentage (x = 0.25) decreases the peak broadness in this regime, as could be seen from **Figure 5.10 (b)**. For Ho-4f state at 11.6 eV (occupied f-orbital in V.B.) this increase in sharpness (less broad) might be related to enhancement in the forbidden transitions as could also be seen from UV-Vis data. Further, intensity corresponding to Ti-3p state at 33 eV is reduced probably associated with a decrease in Ti-3p (33 eV) and O-2s (23 eV) core level electronic interaction as Ti-O bond length increases but since B.E. of Ho-$5p_{1/2}$ state is adjacent to it at 32 eV implies that Ge substitution plays a role in the interaction between them due to the presence of Ge-3d electronic state at 29 eV. Ge concentration enhances Ho-$5p_{3/2}$-O'-2s interaction while suppressing the interaction between Ti-3p state (33 eV)–Ho-$5p_{1/2}$ (32 eV) derived state. $Ho_2Ge_2O_7$ pyrochlore shows exchange splitting of the Ho-4f states due to change in crystal field upon Ti substitution as shown in **Figure 5.10 (a)** and this feature is not seen in the XPS

spectra for lower x (0-0.25) compositions, which might be related to the favoured vibrational level transitions involving $^5F_5$ excited and $^5I_8$ ground electronic states of Ho-4f states present only in tetragonal side of $Ho_2Ge_xTi_{2-x}O_7$ (x=2, 1.9, 1.75, 1.5 and 1). This feature is absent in $Ho_2Ti_2O_7$ due to the difference in the site symmetry of Ho which is D_{3d} relative to D_{5h} in $Ho_2Ge_2O_7$ [66].This splitting in XPS data in the tetragonal side increases from 1.33 to 2.46 eV from x=2 to x=1.9 and then further to 3.72 in x=1.75. The enhancement suggests a possible change in the crystal field potential due to distortion in the GeO_4 tetrahedron. It further distorts the HoO_7 pentagonal bipyramidal associated with the symmetry breaking at the Ho site that increases the luminescence between specific Stark components between the vibrational levels of $^5F_5$ and $^5I_8$ electronic states at 652 nm manifested through photoluminescence data as discussed in next chapter. The strong affinity between O-2s and Ho-$5p_{3/2}$ interaction exists since the binding energies of these states differ only by ~1 eV, having a value of 23 eV and 24 eV, respectively. Ge-3d core state is at 29 eV as mentioned in the XPS data book. XPS peak intensity corresponding to Ho-$5p_{1/2}$ state at 32 eV in $Ho_2Ge_2O_7$, gets increased with change in chemical pressure upon Ti substitution due to strong core level electronic interaction (chemical bond formation) between Ti-3p state and Ho $5p_{1/2}$. It occurs since the B.E. of Ti-3p state is 33 eV almost equal to that of Ho-$5p_{1/2}$ state [93]. This Ti-3p and Ho-$5p_{1/2}$ derived state is markedly seen in total DOS responsible for the change in cross-section of P band with immediate Ti^{4+} substitution in $Ho_2Ti_2O_7$ as shown in **Figure 5.4 (a)** creating agreement between theory and experiment in the form of strong hybridization between Ho $5p_{1/2}$ and Ti-3p orbital.

5.5 Conclusions

The role of chemical pressure upon electronic structure had been investigated in the $Ho_2Ge_xTi_{2-x}O_7$ series of samples. It had been established that subtle variation in the complex dipolar and exchange interaction (J_{nn}/D_{nn} ratio) through the application of chemical pressure changes the electronic structure in such spin ice systems. An excellent match between the experimental and theoretical results of the energy states $Ho_2Ge_xTi_{2-x}O_7$ had been observed. There is a close relationship between the TiO_6 octahedron distortion and the shrinkage effect seen in Ho-O-O' coordination upon Ge^{4+} substitution on the band gap for cubic end of this series. It had been found that band gap as obtained theoretically (DFT calculation) is governed by the 48f oxygen positional parameter. This highlights the role of chemical pressure on the electronic properties of these materials. The symmetry breaking in $Ho_2Ge_2O_7$ (tetragonal pyrogermanate) on alloying with Ti^{4+} is responsible for the 4f splitting of the Ho^{3+} state. Hence for various applications in tuning the band gap, the dependency of the "***x***" (positional parameter) in the $Ho_2Ti_2O_7$ matrix could be taken into account. The band gap can be tuned from 5.249 to 3.744 eV with the variability of Ti inclusion in $Ho_2Ge_2O_7$. Prominent orbital overlap of Ti-3d and O-2p states had also been established. Hybridization between these states plays a crucial role in deciding the band gap of these materials. An excellent match has been established between the experimental data and theoretical calculations of the energy states in $Ho_2Ge_xTi_{2-x}O_7$, highlighting the band gap tenability in this system.